Contents lists available at GrowingScience

Current Chemistry Letters

homepage: www.GrowingScience.com

Quantum simulation of benzothiadiazole-based D-π-A-π-D dyes for enhanced optoelectronic and photovoltaic performance in DSSCs

Zahra Najidi[a,b], Ikram Mennas[b], Badreddine Boukili[b], El Mostafa Benharaf[b], Abdelkhalk Aboulouard[c,d], Mostafa Khouili[a] and Mohammed El idrissi[b*]

[a]*Laboratory of Molecular Chemistry Materials, Catalysis and Environment, Sultan Moulay Slimane University, Beni-Mellal, Morocco*
[b]*Research Team in Sustainable Processes, Advanced Materials and Computational Chemistry, Sultan Moulay Slimane University, Beni-Mellal, Morocco*
[c]*Higher School of Education and Training, Sultan Moulay Slimane University, Beni-Mellal, Morocco*
[d]*Department of Engineering Sciences, Faculty of Engineering and Architecture, Izmir Katip Celebi University, Izmir, Turkey*

CHRONICLE

Article history:
Received January 30, 2026
Received in revised form
March 30, 2026
Accepted June 10, 2026
Available online
June 10, 2026

Keywords:
Dye-sensitized solar cells
Benzothiadiazole derivatives
DFT
TD-DFT

ABSTRACT

In this study, a theoretical investigation of four organically symmetric benzothiadiazole-based D-π-A-π-D dyes (D1–D4) was performed in order to evaluate their potential as photosensitizers in dye-sensitized solar cells (DSSCs). Their structural, electronic, optical, and charge transport properties were analyzed using DFT and TD-DFT methods at the B3LYP/6-31G(d,p) level. Frontier molecular orbital analysis reveals an effective spatial separation between donor and acceptor regions, facilitating intramolecular charge transfer upon photoexcitation. The calculated band gaps range from 2.26 to - 2.60 eV, suggesting that the dyes can absorb light in the visible range, as the LUMO levels (-2.29 to -2.47 eV) are well positioned above the conduction band of TiO_2, allowing for thermodynamically favorable electron injection. The simulated UV-visible spectra show strong absorption bands dominated by HOMO → LUMO excitations, indicating a pronounced intramolecular charge transfer character. The photovoltaic parameters, such as open-circuit voltage, Gibbs free energy of electron injection, and charge transfer rates, indicate efficient electron injection for all dyes, with a particularly promising performance by D1 and D3 due to their high electron affinities and favorable electron transfer, thus validating the potential of these dyes for next generation DSSC applications.

2026 by the authors; licensee Growing Science, Canada.

1. Introduction

In the last few years, the issue of renewable energy has been the subject of extensive scientific research because of the environmental and economic challenges associated with it.[1] The use of fossil-based fuels still represents nearly 80% of the world's energy needs, which leads to a considerable imbalance in their regeneration cycle.[2] This dependence also contributes to the substantial increase in atmospheric greenhouse gas concentrations, which is the primary deliver of global climate change. In this context, it has become a priority to develop new sources of energy.[3] Among them, renewable energies, and more particularly photovoltaic energy, appear to be feasible and sustainable solutions to contemporary energy challenges. It was in this context that Grätzel and O'Regan introduced a new type of photovoltaic cell in 1991: dye-sensitized solar cells (DSSCs). These devices rely on the adsorption of a photosensitive dye onto a nanostructured semiconductor, typically titanium dioxide (TiO_2), enabling the efficient conversion of solar energy into electrical energy. Dye-sensitized solar cells (DSSCs) have attracted significant attention due to their numerous technological and economic advantages. They are distinguished by the low cost of their constituent materials and by simple fabrication processes carried out at low temperatures, which significantly reduce the energy expenses associated with their production.[4,5] In addition to their potential for outdoor solar-energy conversion, DSSCs are particularly attractive for low-light energy harvesting applications owing to their ability to operate efficiently under diffuse illumination and indoor artificial light. This property is not the primary pathway for large-scale energy production, but it significantly broadens the applicability of DSSCs to low-power

* Corresponding author
E-mail address elidrissi.usms@gmail.com (M. E. idrissi)
© 2026 by the authors; licensee Growing Science, Canada
doi: 10.5267/j.ccl.2026.6.003

devices, such as indoor sensors, as well as to diffuse sunlight and indoor artificial lighting. Another major advantage lies in the wide variety of dyes and electrolytes that can be employed, providing considerable flexibility for optimizing their optoelectronic properties[4]. Based on these advantages, extensive research has focused on improving DSSC stability, durability, and efficiency through dye molecular design, electrolyte optimization, and better control of charge injection, separation, transport, and recombination processes.[5] These developments have led to power conversion efficiencies (PCE) exceeding 14.2 %,[6,7] further demonstrating the high potential of this photovoltaic technology. Although PCE values exceeding 14.2% are promising for DSSCs, they remain lower than those reported for conventional polycrystalline silicon solar cells, which typicallyexhibit commercial efficiencies of about 17-20% and certified laboratory efficiencies up to approximately 23.3%.[8] Therefore, although DSSCs do not yet surpass silicon-based technologies in terms of power conversion efficiency, they remain attractive because of their low-cost fabrication, molecular tunability, semi-transparency, and good performance under low-light conditions. In a DSSC, the photosensitizer first absorbs incident light and reaches an excited electronic state. The excited dye then injects an electron into the conduction band of the semiconductor, while the oxidized dye is subsequently regenerated by the redox electrolyte. Therefore, the dye directly controls the main photoelectrochemical steps of the device, including light harvesting, electron injection, and dye regeneration. For this reason, the molecular structure and energy-level alignment of the dye are central factors governing the overall photovoltaic performance of DSSCs.[9,10] In this context, molecular engineering of dyes plays a crucial role in broadening light absorption toward the near-infrared region, improving electron injection, and suppressing charge recombination, thereby enhancing overall photovoltaic performance.[11] The electronic properties of a dye, in both its ground and excited states, govern light harvesting, electron injection into the semiconductor, and dye regeneration. Consequently, the rational design of new dyes increasingly relies on a synergy between experimental synthesis and theoretical modeling. Density functional theory (DFT)-based methods enable the estimation of key ground-state optoelectronic properties prior to synthesis. For organic π-conjugated systems, frontier orbital energies are generally predicted with typical deviations of about 0.1-0.3 eV, depending on the exchange-correlation functional, basis set, and molecular structure.[12] Excited-state properties, including UV–visible absorption spectra, require time-dependent DFT (TD-DFT), which commonly reproduces experimental excitation energies with deviations of approximately 0.2-0.4 eV. These approaches allow the evaluation of energy levels (HOMO and LUMO), excited states, absorption characteristics, dipole moments, and charge-transfer behavior. Among the various molecular designs, D-A-D (donor–acceptor–donor) dyes have attracted increasing attention.[13,14] The symmetrical D-π-A-π-D architecture can favor a more extended and balanced π-electron delocalization along the molecular backbone. This delocalization reduces excessive localization of frontier molecular orbitals and can facilitate electronic transitions with broader visible-light absorption. Moreover, the presence of donor units on both sides of the central acceptor promotes more balanced intramolecular charge transfer from the donor fragments toward the acceptor core upon photoexcitation. Such charge redistribution can improve hole–electron separation and reduce charge recombination. In addition, the more balanced electronic distribution may limit localized charge accumulation and excited-state structural distortion, which contributes to better photophysical stability.[15] Benzothiadiazole-based systems have emerged as particularly promising candidates due to their strong electron-withdrawing character and favorable electronic properties. In particular, D-π-A-π-D architectures incorporating benzothiadiazole units enable efficient intramolecular charge transfer and strong electronic coupling with TiO_2, which improves electron injection and overall device performance.[16-18].

In this setting, our research is focused on systematically looking into how the nature of electron donor and acceptor units, as much as π–conjugation, affect the optical and spectroscopic characteristics of benzothiadiazole-based D-π-A-π-D sensitizers (**Fig 1.**). The objective is to identify structures with a wide absorption range in the visible region, a LUMO level compatible with that of TiO_2 (approximately -4.0 eV), and electronic stability conducive to device longevity.

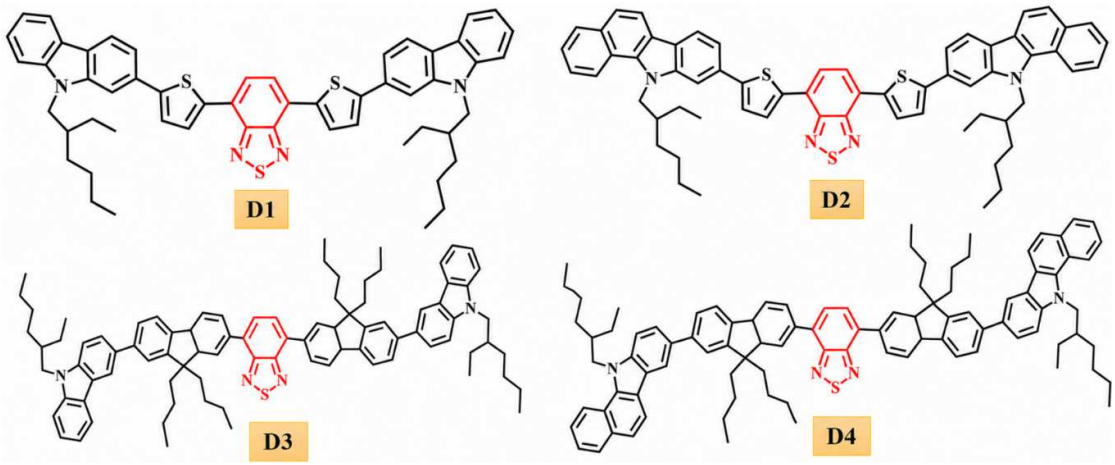

Fig. 1. Chemical structural of dyes (D1-D4)

The equilibrium configurations of the four dyes studied (D1–D4) are shown in Figure 1S, while the Cartesian coordinates of the optimized geometries obtained using TD-DFT/B3LYP/6-31G(d,p) calculations are summarized in Tables

S1–S4. These optimized geometries provide a detailed view of the spatial atomic arrangements of the studied dyes. Nitrogen and sulfur atoms are highlighted because they are part of the donor/acceptor framework and may contribute to the electronic distribution within the conjugated system. Their specific contribution to charge delocalization and intramolecular charge transfer will be discussed later based on frontier molecular orbital (FMO), molecular electrostatic potential (MEP), and PDOS/OPDOS analyses. Analysis of bond lengths and angles within these structures provides insight into factors influencing light harvesting efficiency and optoelectronic performance across the series. Notably, the structural differences observed among the dyes suggest different effects on their respective performance in dye-sensitized solar cell (DSSC) applications.

2. Computational methods

In this study, we performed a computational investigation of a series of four organically symmetric benzothiadiazole-based D-π-A-π-D dyes (D1–D4) employing density functional theory (DFT). All calculations were carried out using the Gaussian 09 package, while GaussView 5.0 was employed for molecular visualization and input preparation.[19,20] The B3LYP/6-31G(d,p) level of theory was chosen because of its balance between computational cost and accuracy, ensuring that all molecules analyzed in this study are treated consistently, and proven reliability in predicting the geometric and electronic properties of organic dyes.[21-24]

The optimal geometries of the dye molecules were verified through vibrational frequency calculations, confirming the absence of imaginary frequencies and demonstrating that all structures correspond to energy minima on the potential surface. Ground-state DFT calculations were used for geometry optimization, frequency analysis, frontier molecular orbital analysis, and electronic-property evaluation. The UV–visible absorption spectra, excitation energies, electronic transitions, and oscillator strengths were calculated using time-dependent DFT (TD-DFT). Origin software was used to plot the simulated absorption spectra. The global chemical reactivity parameters**,** such as electron affinity, ionization potential, chemical hardness, electronegativity, softness, and electrophilicity, were derived from the energies of the frontier HOMO and LUMO orbitals according to the standard DFT relationships.

The chemical potential (μ)**,** which reflects the tendency of electrons to escape from a molecule, is defined as follows:

$$\mu = \frac{(E_{HOMO} + E_{LUMO})}{2} \quad (1)$$

The chemical hardness (η), representing the resistance of a molecule to charge transfer, is expressed as follows:

$$\eta = \frac{(E_{LUMO} - E_{HOMO})}{2} \quad (2)$$

The electronegativity (χ), which indicates a molecule's ability to attract electrons, is given by:

$$\chi = \frac{-(E_{HOMO} + E_{LUMO})}{2} \quad (3)$$

The chemical softness (S), the inverse of hardness and an indicator of molecular polarizability, is calculated as:

$$S = \frac{1}{\eta} \quad (4)$$

Finally, the electrophilicity index (ω), quantifying a molecule's tendency to accept electrons, is defined as:

$$\omega = \frac{\mu^2}{2\eta} \quad (5)$$

These parameters provide a comprehensive description of the reactivity and electronic behavior of the studied molecules, particularly for organic donor molecules employed in organic solar cells (OSCs).[25]

3. Results and discussion

3.1 Analysis of Molecular Frontier Orbitals

The optimal geometries with the respective frontier molecular orbitals (HOMO and LUMO) for the D1 to D4 dye compounds are presented in **Fig**. **2.** The optimized molecules have fairly flat configurations along the length of the conjugated chain, facilitating efficient π electron transfer and efficient intramolecular charge transfer, These variations originate from the electronic effects and spatial positions of the substituent groups, as confirmed by the HOMO/LUMO distributions and the calculated energy gaps.[26] The spatially resolved frontier molecular orbitals provide key information

on the electronic characteristics of the studied dyes. In all of the systems, HOMO is located mainly on the electron donor part, and the HOMO is conjugated to the molecular structure, suggesting that this region is primarily responsible for the occupied electronic state. In comparison, LUMO is primarily distributed over the acceptor part of the molecule, which includes the anchoring unit, pointing to a clear distinction between electron donor and acceptor areas.[27] Such HOMO-LUMO energy distribution implies efficient intra-molecular charge transfer from the donor to the accepter fragment during photoexcitation. This separation of charge is essential for dye-sensitized photovoltaic devices, as it promotes the injection of electrons to the conduction band of the TiO_2 semiconductor. In addition, the extent of orbital overlap varies between D1 and D4, which reflects the impact of molecular structure and conjugation on their electronic properties.

The suitability of dyes D1-D4 for DSSC applications was evaluated using specific energy-alignment criteria. First, the LUMO levels of the dyes should be located above the conduction band edge of TiO_2, usually taken as approximately −4.0 eV, to provide a thermodynamically favorable driving force for electron injection. In the present study, the calculated LUMO energies of D1-D4 range from -2.28 to -2.47 eV, satisfying this requirement. Second, the HOMO levels should allow dye regeneration by the redox electrolyte after electron injection. In addition, the calculated HOMO-LUMO gaps of 2.26-2.60 eV indicate possible absorption in the visible region.[28,29]

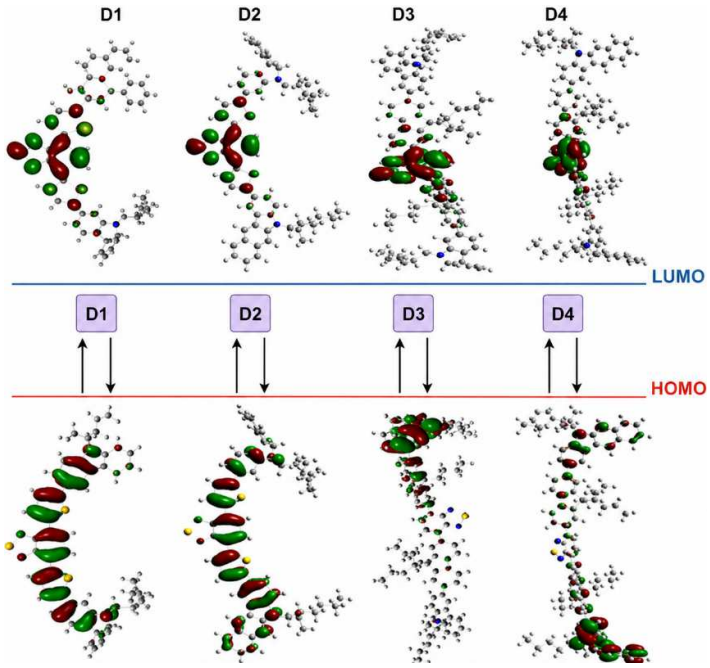

Fig. 2. Spatial distribution for frontier molecular orbitals (HOMO and LUMO) of synthetic dyes D1 to D4, evaluated using TD-DFT calculations.

3.2 Electronic Properties

The **Table 1** below summarizes the main quantum chemical properties of the dyes D1, D2, D3, and D4, as well as TiO_2, to evaluate their energy matching and their suitability for photovoltaic applications. The band gap (Egap) of the dyes varies from 2.2567 to 2.6028 eV, reflecting effective absorption in the visible range. Dye D2 exhibits the lowest band gap, suggesting easier electronic excitation and improved delocalization of the electron density, whereas D3 shows the highest value, indicating enhanced electronic stability.

Table 1. HOMO energy, LUMO energy, energy gap, ionization potential, electron affinity, chemical potential, global hardness, softness, global electrophilicity.

Dyes	**D1**	**D2**	**D3**	**D4**	**TiO_2**
E_{HOMO} (eV)	-4.7217	-4.7299	-4.8891	-4.8736	-7.16
E_{LUMO} (eV)	-2.4425	-2.4732	-2.2863	-2.3056	-4
E_{gap} (eV)	2.2792	2.2567	2.6028	2.568	3.16
IP (eV)	4.7217	4.7299	4.8891	4.8736	7.16
EA (eV)	2.4425	2.4732	2.2863	2.3056	4
μ (eV)	-3.5821	-3.60155	-3.5877	-3.5896	-5.58
***X* (eV)**	3.5821	3.60155	3.5877	3.5896	5.58
η (eV)	1.1396	1.12835	1.3014	1.284	1.58
***S* (eV)**	0.4387	0.4431	0.3842	0.3894	0.3164
ω (eV)	5.6298	5.7478	4.9452	5.0176	9.8532

The LUMO levels of the dyes (−2.2863 at −2.4732 eV) were considerably higher compared to TiO_2 (−4.00 eV), ensuring thermodynamically beneficial electron injection into the semiconductor conduction band. In addition, the HOMO energy levels of the dyes are sufficiently far below that of TiO_2 to prevent the recombination of electrons following injection. The chemical potential (μ) values of the dyes are higher, i.e., less negative, than that of TiO_2, while their electronegativity (χ) values are lower than that of TiO_2. This energy-level difference indicates a favorable tendency for electron transfer from the dyes toward the semiconductor. In addition, the moderate hardness values of the dyes indicate relatively higher electronic reactivity and charge-transfer ability. In contrast, TiO_2 shows a larger HOMO–LUMO gap and a higher global hardness value than the studied dyes, as reported in Table 1. These descriptors, already defined in the Computational methods section, indicate a greater resistance of TiO_2 to electronic excitation and charge transfer, which supports its higher electronic stability. [30,31] Collectively, the energy matching of dyes D1-D4 was assessed based on the position of their LUMO levels relative to the TiO_2 conduction band, their HOMO levels with respect to dye regeneration, and their HOMO-LUMO gaps related to visible-light absorption. The calculated LUMO levels of the dyes, ranging from -2.2863 to -2.4732 eV, are higher than the TiO_2 conduction band edge taken as -4.00 eV, indicating favorable electron injection. In addition, their HOMO-LUMO gaps of 2.2567-2.6028 eV support possible visible-region absorption, indicating suitable energetic alignment for DSSC-related applications.

3.3. Molecular Electrostatic Potential (MEP)

To support the discussion of charge distribution and intramolecular charge transfer (ICT) in the studied dyes, molecular electrostatic potential (MEP) analysis was performed. In the context of DSSCs, MEP mapping is useful for visualizing the polarization between donor and acceptor fragments and for identifying electron-rich regions located near the acceptor/anchoring units, which may favor charge migration toward the semiconductor after photoexcitation. Therefore, the MEP analysis was used here only as a qualitative tool to complement the FMO and TD-DFT results, rather than to investigate general electrophilic/nucleophilic reactivity or hydrogen-bonding interactions. In the MEP maps, red and yellow regions indicate electron-rich areas, blue regions correspond to electron-deficient areas, and green regions represent electronically neutral zones.

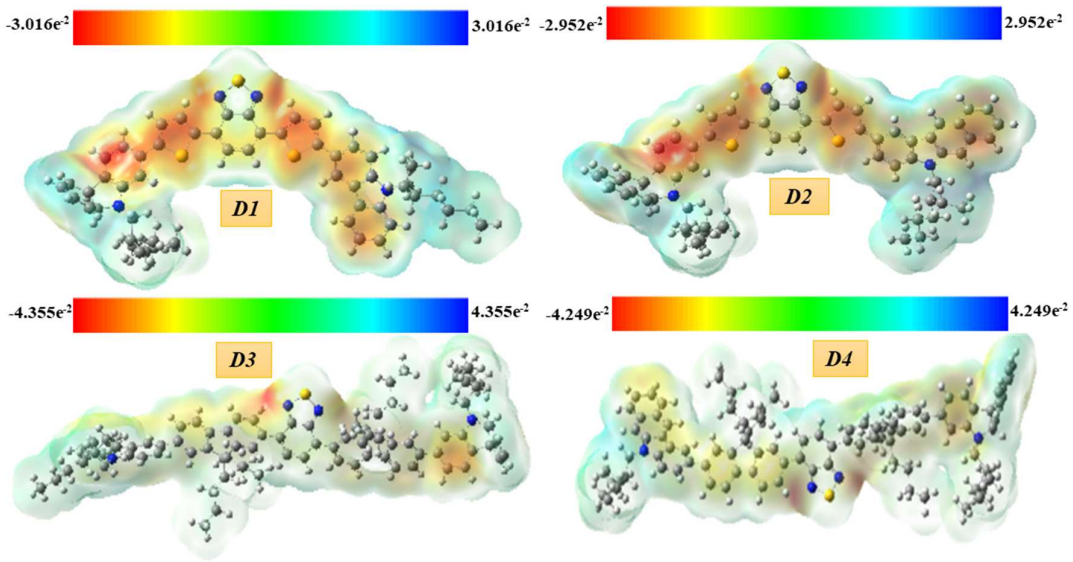

Fig. 3. MEP surface obtained at level B3LYP/6-311 G(d, p) of the compounds D1, D2, D3 and D4.

As shown in Fig. 3, the MEP surfaces reveal a clear charge separation within all dyes. The negative electrostatic potential is predominantly localized over the acceptor and anchoring groups, which constitute the primary sites for adsorption onto the TiO_2 surface and subsequent electron injection. In contrast, the positive potential is concentrated on the electron-donor moieties and alkyl substituents. This spatial charge segregation confirms a strong dipolar character and supports efficient intramolecular charge transfer from donor to acceptor units upon photoexcitation. Such charge redistribution is beneficial for DSSC performance, as it promotes electron injection into TiO_2 while reducing charge recombination at the dye–electrolyte interface.

3.4. Quantum optical analysis TDOS and OPDOS

The electronic structure of organic dyes D1–D4 was analyzed by investigating the total density of states (TDOS), the projected density of states (PDOS), and the overlap population density of states (OPDOS), complemented by the visualization of molecular orbitals using the Multiwfn program (version 3.3.7) developed by Lu and Chen .[32] The TDOS analysis allows the overall distribution of electronic states to be examined, while the PDOS highlights the contribution of

different molecular fragments and types of orbitals types. The OPDOS, meanwhile, provides essential information on the nature of orbital interactions, distinguishing between bonding, non-bonding, and antibonding contributions, which are crucial for understanding charge transfer mechanisms. The calculations were carried out until convergence, with convergence criteria set to 4.5×10^{-4} a.u for the maximum force and 3×10^{-4} a.u for the mean square deviation of the force. To ensure that the optimized geometries correspond to true energy minima on the potential energy surface, a vibrational frequency analysis was performed, confirming the absence of imaginary frequencies for all investigated structures, this validates the optimized geometries and ensures the reliability of the calculated electronic properties relevant to dye-sensitized solar cell (DSSC) applications. The TDOS and OPDOS data are presented and summarized in **Fig. 4**.

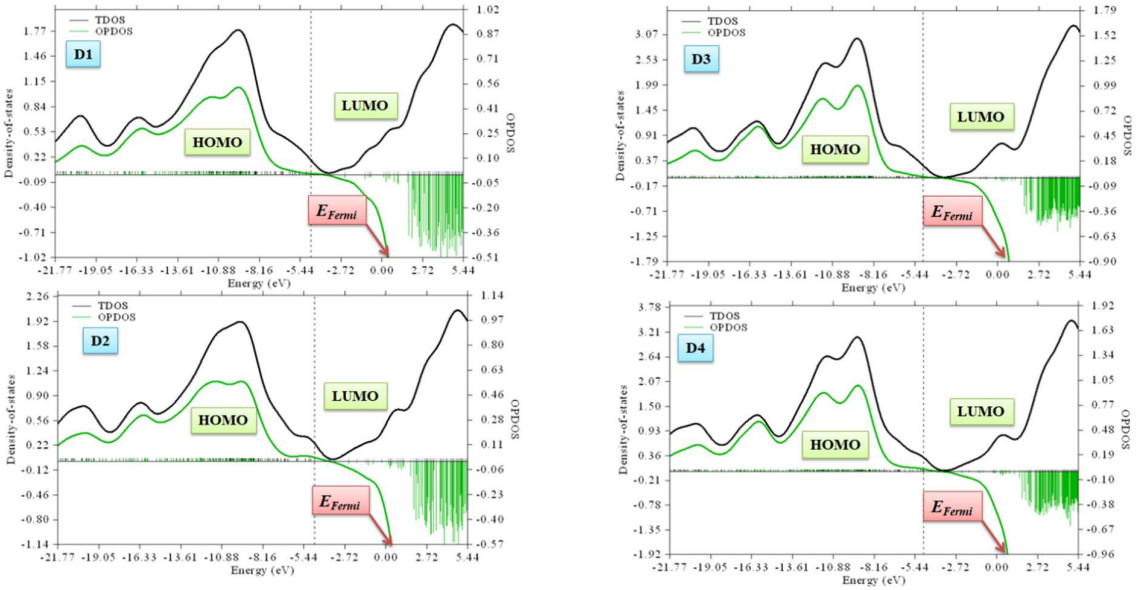

Fig. 4. Analysis of organic dyes D1-D4 through TDOS and OPDOS measurements in relation to the electronic properties for dye-sensitized solar cells.

Fig. 4 represents the TDOS and OPDOS curves of molecules D1 to D4, revealing marked differences in their electronic behavior. The TDOS of D1 has a peak at around 1.77, while D4 has a more pronounced peak at around 3.7, suggesting a greater density of states and enhanced electron availability. Near the Fermi level, the TDOS peaks of the four molecules vary between 0.5 and 1.5, reflecting distinct HOMO and LUMO levels, which are essential for charge transfer. Regarding OPDOS, D1 has a maximum positive value of approximately 0.87 below the Fermi level, while D4 reaches nearly 1.9, highlighting greater constructive orbital overlap, which is favorable for electronic stability and electron transport. Above the Fermi level, the OPDOS becomes negative, with values up to -0.5 for D1 and close to -0.9 for D4, indicating more pronounced antibonding interactions in the unoccupied orbitals. Thus, D4, with its larger TDOS and more intense OPDOS in the HOMO region, suggests a higher electron transport potential compared to D1, which may translate into better photovoltaic performance. These TDOS and OPDOS results provide a comparative description of the electronic structure and orbital interactions within the D1–D4 series. Although no universal reference threshold is available for directly converting TDOS/OPDOS intensities into photovoltaic efficiency, the relative differences observed among the dyes suggest that stronger density of states near the frontier orbital region and more favorable orbital overlap may support improved charge-transfer ability.

Upon photoexcitation, the HOMO is primarily localized on the donor and π-conjugated bridge, while the LUMO concentrates on the acceptor and anchoring units, promoting efficient intramolecular charge separation. PDOS and frontier orbital analyses indicate that nitrogen and sulfur atoms contribute to the electronic distribution within the acceptor segment of the dyes. Their contribution supports charge delocalization along the conjugated framework and participates in the intramolecular charge-transfer character observed upon excitation. However, a rigorous description of electronic coupling with TiO_2 would require explicit interfacial modeling of the dye/TiO_2 system.

3.5 UV-VIS Absorption properties

The simulated UV–Visible absorption spectra of dyes D1–D4, calculated at the TD-DFT/B3LYP/6-31G(d,p) level, exhibit absorption bands within the visible region. These results suggest that the studied dyes may possess favorable light-harvesting characteristics, which represent only one of the requirements for DSSC sensitizers. However, experimental device fabrication and photovoltaic measurements are required to confirm their practical suitability in complete DSSC devices. The dominant electronic transitions are mainly attributed to HOMO → LUMO excitations, reflecting effective intramolecular charge transfer (ICT) between the donor and acceptor moieties of the dyes. Among the investigated systems,

D2 exhibits the most red-shifted and intense absorption profile, suggesting enhanced π-conjugation and stronger electron delocalization. In contrast, D3 and D4 display absorption maxima at shorter wavelengths, corresponding to relatively higher transition energies. These spectral variations are mainly associated with the nature and position of the functional groups governing the ICT process. In addition, the broader visible and near-infrared absorption regions observed for D1 and D2 suggest improved solar light harvesting capability compared with the other dyes.[33]

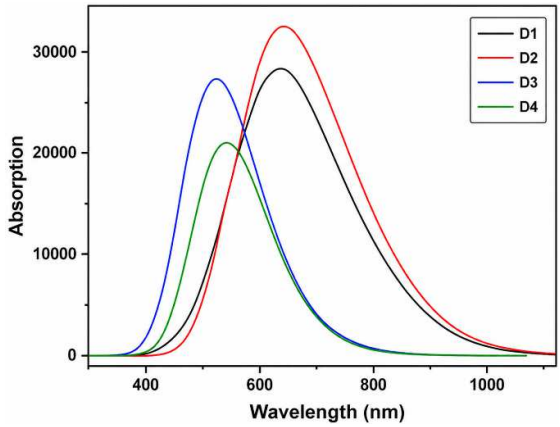

Fig. 5. Simulated UV-visible absorption of all compound at the TD-DFT B3LYP/6-31 G(d,p) level.

3.6. Photovoltaic proprieties

The power conversion efficiency (PCE) is a commonly used parameter for evaluating DSSC performance and is generally expressed as a function of the short-circuit current density (Jsc), open-circuit voltage (Voc), fill factor (FF), and incident power density (Pinc), as shown in Eq. 6.[34] However, no explicit PCE calculations were carried out in the present study.

$$\boldsymbol{PCE = \frac{J_{SC} \times V_{OC} \times FF}{P_{Inc}}} \quad (6)$$

Among these, the open-circuit voltage (Voc) is influenced by the energy level difference between the LUMO of the dye and the conduction band of the TiO_2 semiconductor. The theoretical values of V_{oc} can be estimated using Eq.7[35]:

$$\boldsymbol{V_{OC} = E_{LUMO} - E_{CB}} \quad (7)$$

where E_{LUMO} is the LUMO energy of the dye and E_{CB} corresponds to the conduction band edge of TiO_2, typically taken as –4.0 eV vs. vacuum. According to **Table 2**, the theoretical Voc values for dyes range from 1.5268 to 1.7137 eV, indicating a sufficient driving force for efficient electron injection into the TiO_2 conduction band.[36] The short-circuit current density (J_{sc}) can be estimated by Eq. (8),

$$\boldsymbol{J_{SC} = \int LHE(\lambda) \times \emptyset_{inj} \times \eta_{coll} d\lambda} \quad \textbf{(8)}$$

where, *LHE(λ)* is the light harvesting efficiency at a given wavelength, $\emptyset_{inj}$ is the electron injection efficiency, and η_{coll} is the charge collection efficiency, often considered constant when using the I^-/I_3^- redox couple. The efficiency of electron injection can be further assessed using the Gibbs free energy change (ΔG_{inject}) of electron injection from the excited dye into TiO_2, calculated as follows[37]:

$$\boldsymbol{\Delta G_{inject} = E^*_{dye} - E_{CB}} \quad (9)$$

where E_{dye} is the excited state oxidation potential of the dye,[38] defined as:

$$\boldsymbol{E^*_{dye} = E_{dye} - E_{00}} \quad (10)$$

where $E_{dye} \approx -E_{HOMO}$ and E_{00} represents the vertical excitation energy associated with λ_{max}.

The calculated values (**Table 2**) show that ΔG_{inject} is negative for all dyes (from -1.203 to -1.422 eV), confirming that the excited state of the dye lies energetically above the TiO_2 conduction band. This ensures spontaneous electron injection, a key requirement for high J_{sc} values.

Table 2. Photovoltaic performances of the studied dyes.

Dyes	HOMO (eV)	LUMO (eV)	E_{gap}(eV)	V_{oc}(eV)	ΔG_{inject}
D1	-4.7217	-2.4425	2.2792	1.5575	-1.229
D2	-4.7299	-2.4732	2.2567	1.5268	-1.203
D3	-4.8891	-2.2863	2.6028	1.7137	-1.422
D4	-4.8736	-2.3056	2.5680	1.6944	-1.412

An analysis of the frontier molecular orbital energy (HOMO and LUMO) along with essential photovoltaic parameters such as the energy gap (E_{gap}), open-circuit voltage (V_{oc}), and Gibbs free energy change for injection (ΔG_{inject}), shows that all four dyes studied possess strong electronic properties suitable for application in DSSCs. The LUMO levels, which range from -2.28 to -2.47 eV, sit above the TiO_2 conduction band edge, making efficient electron injection. Meanwhile, the HOMO levels (–4.72 to –4.89 eV) are positioned below the redox potential of the I^-/I_3^- electrolyte, which helps with efficient dye regeneration. The energy gaps we calculated (2.26–2.60 eV) point to good light absorption in the visible spectrum, and the negative ΔG_{inject} values (–1.20 to –1.42 eV) show that electron injection happens spontaneously. Moreover, D3 and D4 stand out with better energy alignments and higher V_{oc} values, hinting at a slight edge in photovoltaic performance.

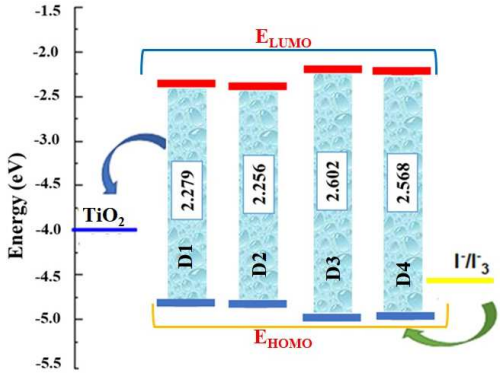

Fig. 6. Diagram of the computed energy level of the sensitizers using B3LYP/6-31G(d,p) method.

Additionally, the light harvesting efficiency (LHE) is directly related to the oscillator strength (*f*)[39] through Eq. (11):

$$LHE = 1 - 10^{-f} \quad (11)$$

Table 3. Assignment of Molecular Orbitals Involved in Electronic Transitions, Together with Maximum Absorption Wavelengths (λmax), Excitation Energy, and (LHE) Corresponding Excitation Energies and Oscillation Forces (f) for all Dyes Studied

Dyes	Transition	E_{ex}(eV)	λ (nm)	F	LHE
D1	HOMO → LUMO (99%)	1.9512	641.28	0.7629	0.8273
	HOMO-1 → LUMO (95%)	2.222	557.93	0.00229	0.0052
	HOMO-2 → LUMO (47%)	2.361	525.11	0.0124	0.0281
D2	HOMO → LUMO (98%)	1.9334	641.2754	0.7629	0.8273
	HOMO-1 → LUMO (95%)	2.2222	557.9344	0.0229	0.0513
	HOMO-2 → LUMO (47%)	2.3611	525.112	0.0124	0.0281
D3	HOMO → LUMO (74%)	2.3112	536.4494	0.4854	0.6729
	HOMO-1 → LUMO (78%)	2.4468	506.7198	0.1541	0.2987
	HOMO-2 → LUMO (92%)	2.7183	456.1093	0.0891	0.1852
D4	HOMO → LUMO (77%)	2.286	542.363	0.4927	0.6784
	HOMO-1 → LUMO (54%)	2.3791	521.1391	0.0177	0.0399
	HOMO → LUMO+1 (39%)	2.393	518.112	0.0087	0.0198

3.7. Charge Transport and Charge Transfer

The transfer integral (t) reflects electronic coupling through frontier orbital overlap, where higher values indicate stronger coupling and more efficient charge transfer. In organic semiconductors, reported benchmark values range from <1 meV (weak coupling) to several tens of meV (moderate to strong coupling), with values >~50 meV corresponding to strong electronic interactions and efficient charge transport. [40-42]

These references were used to classify the coupling strength in this study. This integral can be calculated using a specific equation and Koopman's theorem, which relates orbital energies to ionization potentials and electron affinity. This gives us valuable insight into how molecules couple electronically and how efficiently charges can move. To compute the charge transfer integrals for electrons and holes, we rely on these relationships.[43]

$$t_{electron} = \frac{1}{2}(E_{LUMO+1} - E_{LUMO}) \quad (12)$$

$$t_{hole} = \frac{1}{2}(E_{HOMO} - E_{HOMO-1}) \quad (13)$$

In this context, E_{LUMO} and E_{HOMO} refer to the energies of the lowest and highest occupied molecular orbital, while E_{LUMO+1} and E_{HOMO-1} are the energies of the immediately higher and lower molecular orbitals. The rearrangement energy (λ) is divided into two parts, internal (λ_{int}) and external (λ_{ext}), which are related to structural changes within the molecule and outside influences from the environment. In our work, we disregard the external part and focus solely on λ_{int}. We compute the internal reorganization energies for electrons ($\lambda_{electron}$) or holes (λ_{hole})[44] as follows:

$$\lambda_{electron} = [E_0^{anion} - E_{anion}] + [E_{anion}^0 - E_0] \quad (14)$$

$$\lambda_{hole} = [E_0^{cation} - E_{cation}] + [E_{cation}^0 - E_0] \quad (15)$$

The neutral molecule's energy in its optimized fundamental state is denoted as E_0, the energies of the optimized cation and anion are referred to as E_{cation} and E_{anion}. E_0^{anion} and E_0^{cation} represent the neutral energy at the optimized anion and cation geometry. E_{anion}^0 and E_{cation}^0 represent the anion energy and cation energy at the optimized neutral geometry.

The charge transfer rate (k_{CT}) is subsequently estimated from the energy of reorganization and the integral of the charge transfer using Marcus theoretical model[45]:

$$K_{ct}^{hol/elec} = \left(\frac{\pi}{\lambda^{hol/elec} K_B T}\right)^{1/2} \frac{t_{hol/elec}^2}{h} e^{\left(\frac{\lambda^{hol/elec}}{4K_B T}\right)} \quad (16)$$

where k_B represents Boltzmann's constant, T is the absolute temperature (298 K), h is Planck's reduced constant, t is the electronic couplage (charge transfer integral) among two molecules, as well as λ is the reorganization's energy.

Table 4. Charge transport rates and transfer of charge integrals computed at TD-DFT B3LYP/6-31G(d,p) level,

Dyes	t_{hole}(eV)	t_{elec}(eV)	λ_{ele}(eV)	λ_{hole}(eV)	k_{CT}^{ele} (s^{-1})	k_{CT}^{hole} (s^{-1})
D1	0.165	0.652	0.183	0.324	$4.62*10^{13}$	$1.22*10^{13}$
D2	0.121	0.283	0.225	0.398	$6.84*10^{12}$	$9.53*10^{11}$
D3	0.071	0.590	0.206	0.248	$3.87*10^{13}$	$1.87*10^{12}$
D4	0.020	0.224	0.276	0.345	$1.22*10^{12}$	$2.46*10^{11}$

Table 4 summarizes the charge transfer integrals (t_{hole} and $t_{electron}$), internal reorganization energies (λ_{hole} and $\lambda_{electron}$), and charge transfer rates (k_{CT}) for the organic dyes D1–D4, calculated at the TD-DFT B3LYP/6-31G(d,p) level. The $t_{electron}$ values indicate that D1 and D3 exhibit strong electronic coupling (0.652 and 0.590 eV), suggesting highly efficient electron transport, whereas t_{hole} is generally lower, particularly for D4 (0.020 eV), implying limited hole mobility. The internal reorganization energies reflect molecular rigidity: low values, as observed for D1 and D3, facilitate charge transfer, while higher values for D2 and D4 hinder mobility. [43,46,47] The calculated charge transfer rates (k_{CT}^{ele} and k_{CT}^{hole} confirm these trends, with D1 and D3 reaching very high electron transfer rates (~10^{13} s^{-1}) and lower hole transfer rates, especially for D4 (~10^{11} s^{-1}). These results indicate that D1 and D3 are the most efficient dyes for electron transport, while hole transport remains less favorable across all dyes and is particularly limited for D4. This analysis highlights the importance of maximizing electronic coupling and minimizing internal reorganization to enhance DSSC performance. Overall, these trends provide direct insight into the charge transport capabilities of the molecules and can guide the design of more efficient dyes for photovoltaic applications.

4. Transition Density Matrix (TDM) and hole–electron isosurface analysis

Fig. 7 illustrates the Transition Density Matrix (TDM) analysis and hole–electron isosurfaces of the investigated dyes. TDM analysis provides valuable insight into electron excitation processes, intramolecular charge-transfer (ICT) behavior, and exciton dissociation within molecular systems. In particular, the TDM maps reveal the electronic interactions between donor and acceptor fragments by identifying the redistribution of electron density upon photoexcitation. Local excitation states appear mainly along the diagonal regions, whereas off-diagonal contributions indicate charge-transfer excitations associated with electron–hole coherence and effective charge separation.[48,49] Complementarity, the hole–electron isosurface analysis visualizes the spatial distribution of holes and electrons in the excited states, allowing identification of preferred charge-transfer pathways and evaluation of the localization or delocalization character of the excitations.[50,51] Parameters such as the average hole–electron distance and overlap index further quantify the extent of charge transfer within the sensitizers. Overall, these analyses provide qualitative information on the excited-state charge redistribution properties of the isolated dye molecules. However, a rigorous description of electron injection into TiO_2 would require explicit interfacial modeling of the dye/TiO_2 system to account for surface interactions.

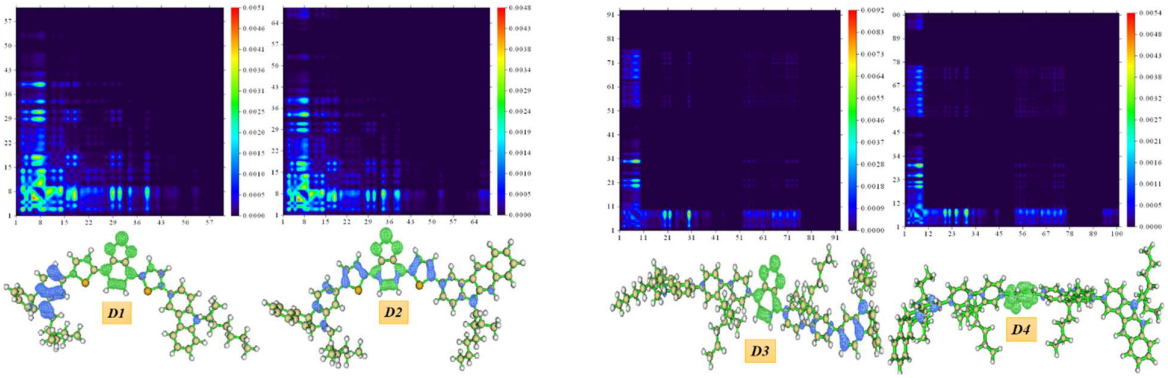

Fig. 7. Transition Density Matrix (TDM) and hole–electron isosurface analysis of (D1-D4)

The transition density matrices (TDM) for molecules D1 to D4 show the nature of the electronic excitations by clearly distinguishing localized states from charge transfer states. The strong intensities along the diagonal observed for D1 and D2 indicate localized excitations, where the electron remains close to the hole, thus limiting charge separation. In contrast, D3 and D4 show more pronounced off-diagonal regions, indicating significant charge transfer between distinct molecular fragments, promoting better hole-electron separation. This distinction is further confirmed by the analysis of hole-electron isosurfaces: D1 and D2 exhibit overlapping spatial distributions of holes and electrons, reflecting localized excitation, while D3 and D4 exhibit a clear separation between charges, characteristic of charge transfer states. This effective separation is crucial for exciton dissociation and improved performance in optoelectronic and photovoltaic devices. Thus, the joint study of TDM and isosurfaces highlights the fundamental impact of structural modifications on electronic behavior, guiding the design of materials with optimized properties for charge transport and separation.

5. Conclusion

This study systematically evaluates the electronic, optical, and charge-transport properties of four benzothiadiazole-based D-π-A-π-D organic dyes (D1-D4) as potential photosensitizers for dye-sensitized solar cells (DSSCs). Analysis of carrier dynamics reveals that electron transport is more favorable than hole transport across the series, particularly for D1 and D3. This behavior can be attributed to their stronger electronic coupling constants and lower reorganization energies, which may facilitate electron mobility within the studied molecular series. The calculated HOMO-LUMO gaps of 2.26-2.60 eV suggest electronic transitions in an energy range that may be compatible with visible-light absorption. However, the efficiency and intensity of light absorption cannot be assessed from the band gap alone. Therefore, the optical behavior was further evaluated using TD-DFT results, including absorption wavelengths, oscillator strengths, light-harvesting efficiency, and excited-state configurations, which together provide a more reliable description of the absorption properties of the studied dyes. The observed variations in the HOMO-LUMO gaps can be related to differences in π-conjugation, donor–acceptor distribution, and the electronic effects of the substituents, as reflected by the frontier orbital distributions. The LUMO energy levels of the dyes, ranging from -2.29 to -2.47 eV, are positioned above the TiO_2 conduction band edge, suggesting a thermodynamically favorable driving force for electron injection. The computed open-circuit voltages (V_{OC}) indicate favorable energetic alignment for DSSC-related applications, particularly for D3 and D4. However, these results should be considered as theoretical indicators rather than definitive proof of device performance, since experimental DSSC fabrication, photovoltaic measurements, and explicit dye/TiO_2 interfacial studies would be required for full validation. Overall, the results suggest that structural variations within this limited benzothiadiazole-based dye series can influence the calculated optoelectronic and charge-transfer descriptors. These findings provide preliminary theoretical guidance for the rational design of related DSSC dyes, while emphasizing the need for future experimental and interfacial dye/TiO_2 investigations to confirm their practical photovoltaic performance.

References

1. Boro B., Gogoi B., Rajbongshi B.M., Ramchiary, A. **(2018)** Nano-structured TiO2/ZnO nanocomposite for dye-sensitized solar cells application: A review. *Renew. Sustain. Energy Rev.* 81, 2264–2270. https://doi.org/10.1016/j.rser.2017.06.035
2. Aboulouard A., Altunkum D., Şaş E.B., Bensemlali M., Can M., Nasrellah H., El idrissi M. **(2023)** Experimental and computational study of triphenylamine dyes for photovoltaic cell applications. *The European Physical Journal Applied Physics*, *98*, 17. https://doi.org/10.1051/epjap/2023220283
3. Kaliramna S., Dhayal S.S, R., Khaturia S., Ameta K.L., Kumar, N. **(2022)** A review and comparative analy., Chaudhary sis of different types of dyes for applications in dye-sensitized solar cells. *Brazilian Journal of Physics*, *52*(4), 136. https://doi.org/10.1007/s13538-022-01109-4
4. Abdelkhalk A., Mustafa C., Benachir E., El idrissi M,. Laasri S. **(2023).** A computational study of thiophene containing small-molecule electron acceptors for non-fullerene organic photovoltaic cells. *Mater. Sci. Energy Technol.* 6, 137–144. https://doi.org/10.1016/j.mset.2022.12.007

5. Hnawi, S. K. **(2022)** Investigation of Aloe Vera latex used as natural dye in TiO2-based heterojunction and liquid-electrolyte dye-sensitized solar cells. *J. Sol. Energy Eng.* 144, 051002.
6. Mathew S.; Yella A.; Gao P., Humphry-Baker R., Curchod B.F.E., Ashari-Astani N., Tavernelli I., Rothlisberger U., Nazeeruddin M.K., Grätzel M. (**2014)** Dye-sensitized solar cells with 13% efficiency achieved through the molecular engineering of porphyrin sensitizers. *Nature Chemistry*, 6, 242–247.
7. Kakiage K., Aoyama Y., Yano T., Oya K., Fujisawa J. I., Hanaya M. **(2015)**. Highly-efficient dye-sensitized solar cells with collaborative sensitization by silyl-anchor and carboxy-anchor dyes. *Chemical communications*, *51*(88), 15894-15897. https://doi.org/10.1039/C5CC06759F
8. Hara K. Suga S., Katoh R., Furube A., Dan-oh Y., Tachiya M., Shinpo A., Sato T. **(2003) ,**Significant improvement of photovoltaic performance in dye-sensitized solar cells based on novel indoline dyes. *Journal of Physical Chemistry B*, , 107 (20), 597–606.
9. Green M., Dunlop E., Yoshita M. **(2026)** Solar Cell Efficiency Tables. *Progress in Photovoltaics: Research and Applications.* 34(4), 482–496, https://doi.org/10.1002/pip.70068.
10. Chauhan, R. **(2022)** Scanning prevalent technologies to promote scalable devising of DSSCs: An emphasis on dye component precisely with a shift to ambient algal dyes. *Inorg. Chem. Commun.* 139, 109368.
11. Brabec C.J., Heeney M., McCulloch I., Nelson, J. **(2011)** Influence of blend microstructure on bulk heterojunction organic photovoltaic performance. *Chem. Soc. Rev.* 40, 1185–1199
12. Ghosh S., Yadav V.K., Mukherjee V. **(2019**) Impact of environmental factors on photovoltaic performance and their mitigation strategies–A holistic review. *Renewable Energy Focus*, *28*, 153-172. https://doi.org/10.1016/j.ref.2018.12.005
13. Jathar L. D. **(2023)**Comprehensive review of environmental factors influencing the performance of photovoltaic panels: Concern over emissions at various phases throughout the lifecycle. *Environ. Pollut.* **326**, 121474.
14. Arif A., Aboulouard A., Can M., Bensemlali M. Boulghalat M., El idrissi M. **(2023)** Computational study of the optical and photovoltaic properties of novel dyes for dye-sensitized solar cell applications. *Matér. Tech.* **111**, 501.
15. Boukili B., Menas I., Arif A., Kadour Atouailaa M., Aboulouard A., Abdessamad T., El idrissi M. **(2025)** TD-DFT Screening of Acrylic-Based Organic D-Π-A Dye Molecules for Reliable and Highly Efficient Dye-Sensitized Solar Cells. *Physical Chemistry Research*, *13*(3), 545-556. https://doi.org/10.22036/pcr.2025.522084.2681
16. Baron T. **(2021)** *Conception et synthèse de colorants sélectifs du proche infrarouge pour des applications en cellules solaires hybrides transparentes et incolores ainsi que pour la production d'hydrogène* (Doctoral dissertation, Université de Nantes).
17. Hnawi S. K. **(2021)** Investigation of the structura

l, optical, electrical, and dielectrical properties of aloe vera leaf exudate. *J. Sol. Energy Eng.* **143**, 021006.

18. Ouhrir J., Mekaoui Y., Mennas I., Taj S., **El idrissi M..** Manaut B. **(2025).** Exploring the optoelectronic and photovoltaic potential of Spiro-OMeTAD derivatives through quantum chemical investigations. *Current Chemistry Letters.* 14. https://doi.org/10.5267/j.ccl.2025.7.001.
19. Diany R., Kerraj S., Atouailaa M.K., Arif A., Aboulouard A., Boulghalate M., Salah M., El idrissi M. **(2025)** Enhancing the electronic and optical performance of dye-sensitized solar cells with alizarin-based dyes: DFT/TDDFT investigations. *Current Chemistry Letters,* 14. https://doi.org/10.5267/j.ccl.2025.2.006
20. Aboulouard A., Demir N., Can M., El idrissi M. **(2023)** Electronic and optical aspects of novel quinoxaline derivatives as electron donor materials for bulk heterojunction solar cells. *Journal of Molecular Graphics and Modelling*, *121*, 108462. https://doi.org/10.1016/j.jmgm.2023.108462
21. Anthony W.O., Abubakar M.K., Obiyenwa K.G., Abdulsalami I.O., Salaw O.W., Semire B. **(2025)** Computational design of phenoxazine and phenothiazine dye sensitizers with improved charge separation for application in DSSCs: a DFT study, *Discov. Chem*. 2, 263. https://doi.org/10.1007/s44371-025-00352-3.
22. Vuai S.A.H., Khalfan M.S., Babu N.S. **(2021)** DFT and TD-DFT studies for optoelectronic properties of coumarin based donor-π-acceptor (D-p-A) dyes: applications in dye-sensitized solar cells (DSSCS), *Heliyon.* 7. https://doi.org/10.1016/j.heliyon.2021.e08339.
23. Bora S.R., Barman B., Kalita D.J. (2025) Theoretical design and analysis of D–π–A–A′ organic dyes for enhanced efficiency in DSSCs by modifying donor (D) and acceptor (A) moieties, *RSC Adv.* 15, 42099–42112. https://doi.org/10.1039/D5RA07258A.
24. Aboulouard, A., Atouailaa, M. K., Elhadadi, B., Bensemlali, M., Boulghallat, M., Laasri, S. El idrissi, M. (2022). A theoretical study of non-fullerene electron acceptor-based on thiophene derivatives for organic solar cells. *Materials Today: Proceedings,* 66, 329-334.
25. Mehboob M. Y. **(2021)** Designing of benzodithiophene core-based small molecular acceptors for efficient non-fullerene organic solar cells. *Spectrochim. Acta. A. Mol. Biomol. Spectrosc.* 244, 118873
26. Kerraj S., Arif A., rachdi Y., Aboulouard A., Salah M., El idrissi M., Said Belaaouad. **(2025)**Exploring the Optoelectronic and Photovoltaic Properties of Ru-Arene Complexes: DFT and TD-DFT Insights into DSSC Performance. Journal of Organometallic Chemistry, 123650. https://doi.org/10.1016/j.jorganchem.2025.123650.
27. Gómez, S., Giovannini, T. & Cappelli, C. Absorption spectra of xanthines in aqueous solution: A computational study. *Phys. Chem. Chem. Phys.* **22**, 5929–5941 (2020).
28. Hagfeldt, A.; Boschloo, G.; Sun, L.; Kloo, L.; Pettersson, H. Dye-sensitized solar cells. Chem. Rev. 2010, 110 (11), 6595–6663.

29. Mathew, S. et al. Dye-sensitized solar cells with 13% efficiency achieved through the molecular engineering of porphyrin sensitizers. Nat. Chem. 2014, 6, 242–247.
30. Yu A.Y., Efil K., Yang R. Hu Q.M. **(2015)** A Comprehensive Theoretical Investigation of the Molecular Properties of Methyl Bromide (CH_3 Br). *Z. Für Naturforschung A* 70, 1025–1030.
31. Ding W.L., Wang D.-M., Geng Z.-Y., Zhao X.-L., Xu W.-B. **(2013)** Density functional theory characterization and verification of high-performance indoline dyes with D–A–π–A architecture for dye-sensitized solar cells. *Dyes Pigments* , 98, 125–135.
32. Lu T., Chen F. **(2012)** Multiwfn: A multifunctional wavefunction analyzer. *J. Comput. Chem.* 33, 580–592.
33. Abdellah I.M., Koraiem A.I., El-Shafei A. **(2019)** Structure-property relationship of novel monosubstituted Ru (II) complexes for high photocurrent and high efficiency DSSCs: Influence of donor versus acceptor ancillary ligand on DSSCs performance. *Sol. Energy* 177, 642–651.
34. Hassan T., Adnan M., Hussain R., Hussain F., Khan M.U. **(2023)**Molecular engineering of Pyran-fused acceptor–donor–acceptor-type non-fullerene acceptors for highly efficient organic solar cells—A density functional theory approach. *J. Phys. Org. Chem.* 36, e4507.
35. Zhang J. **(2012)** Density functional theory characterization and design of high-performance diarylamine-fluorene dyes with different π spacers for dye-sensitized solar cells. *J. Mater. Chem.* 22, 568–576.
36. Zhang J., Li H. B., Sun S. L., Geng Y., Wu Y., Su Z. M. **(2012)** Density functional theory characterization and design of high-performance diarylamine-fluorene dyes with different π spacers for dye-sensitized solar cells. *Journal of Materials Chemistry,* 22(2), 568-576.
37. Kerraj S., Salah M., Chtita S., El idrissi M., Belaaouad S., Mohammed M., Komiha N. **(2022)** Theoretical study of photovoltaic performances of Ru, Rh and Ir half sandwich complexes containing N, N chelating ligands in Dye-Sensitized Solar Cells (DSSCs). DFT and TD-DFT investigation. *Computational and Theoretical Chemistry*, *1209*, 113630. https://doi.org/10.1016/j.comptc.2022.113630
38. Ryu S. **(2014)** Voltage output of efficient perovskite solar cells with high open-circuit voltage and fill factor. *Energy Environ. Sci.* **7**, 2614–2618.
39. Zhang J. **(2012)** Density functional theory characterization and design of high-performance diarylamine-fluorene dyes with different π spacers for dye-sensitized solar cells. *J. Mater. Chem.* **22**, 568–576.
40. Troisi, A. **(2007)** Charge transport in high mobility organic semiconductors. *Chem. Soc. Rev.,* 36, 1972–1989.
41. Coropceanu, V. **(2007)** Charge transport in organic semiconductors. *Chem. Rev.,* 107, 926–952.
42. Deng and Goddard. **(2004)** Electronic coupling and charge transport in organic systems. *J. Phys. Chem. B.,* 108, 8614–8621.
43. Brédas J.-L., Beljonne D., Coropceanu V. Cornil J. **(2004)** Charge-Transfer and Energy-Transfer Processes in π-Conjugated Oligomers and Polymers: A Molecular Picture. *Chem. Rev.* 104, 4971–5004.
44. Aboulouard A., Jouaiti M., El idrissi M. **(2026)** Simulation Analysis of Dye-Sensitized Photovoltaic Cells Performance Using Three Moroccan Natural Dyes. *Progress in Color Colorants Coating,* 19**,** 37-45. https://doi.org/2010.30509/pccc.2025.167563.1400
45. Gong M., Zeng L., Wang W., Dong X., Yu Z., Wang S., Yang Y. **(2024)** Effects of several auxiliary acceptors and anchoring groups on charge transfer and photophysical properties of D-A π-A type DSSCs: a DFT study, *J. Fluor.* 35 2285–2297, https://doi.org/10.1007/s10895-024-03685-x.
46. Brédas, J.L., Calbert, J. P., da Silva Filho, D. A., Cornil, J. **(2002)** Organic semiconductors: A theoretical characterization of the basic parameters governing charge transport. *Proceedings of the National Academy of Sciences.*, **99**, 5804–5809. https://doi.org/10.1073/pnas.092143399
47. Shuai Z., Li W., Ren J., Jiang Y., Geng H. **(2020)** Applying Marcus theory to describe the carrier transports in organic semiconductors: limitations and beyond. *The Journal of Chemical Physics.*, 153, 080902. https://doi.org/10.1063/5.0018312
48. Taouali W., Alimi K. **(2024)** Optimizing non-fullerene acceptor molecules constituting f luorene core for enhanced performance in organic solar cells: a theoretical methodology, J. Mol. Model 30, 342, https://doi.org/10.1007/s00894-024-06120-x.
49. P. Grobas Illobre. **(2021)** Time-Resolved Excited-State Analysis of Molecular Electron Dynamics, Journal of Chemical Theory and Computation. Analyse dynamique des transitions électroniques et visualisations associées.
50. Masood T.B., Thygesen S.S., Linares M., Abrikosov A.I., Natarajan V., Hotz I. **(2021)** Visual analysis of electronic densities and transitions in molecules. In *Computer Graphics Forum* 40(3), 287-298. https://doi.org/10.1111/cgf.14307
51. Zou X. **(2020)** An Insight into the Excitation States of Small Molecular Systems Using Natural Transition Orbitals and Hole–Electron Distribution Analysis, *Molecules*, 25.

© 2026 by the authors; licensee Growing Science, Canada. This is an open access article distributed under the terms and conditions of the Creative Commons Attribution (CC-BY) license (http://creativecommons.org/licenses/by/4.0/).